SIAM J. Applied Dynamical Systems
Vol. 8, No. 2, pp. 527–553

Nonlinear Drillstring Dynamics Analysis*

Christophe Germay†, Nathan Van de Wouw‡, Henk Nijmeijer‡, and Rodolphe Sepulchre†

Abstract. This paper studies the dynamical response of a rotary drilling system with a drag bit, using a lumped parameter model that takes into consideration the axial and torsional vibration modes of the bit. These vibrations are coupled through a bit-rock interaction law. At the bit-rock interface, the cutting process introduces a state-dependent delay, while the frictional process is responsible for discontinuous right-hand sides in the equations governing the motion of the bit. This complex system is characterized by a fast axial dynamics compared to the slow torsional dynamics. A dimensionless formulation exhibits a large parameter in the axial equation, enabling a two-time-scales analysis that uses a combination of averaging methods and a singular perturbation approach. An approximate model of the decoupled axial dynamics permits us to derive a pseudoanalytical expression of the solution of the axial equation. Its averaged behavior influences the slow torsional dynamics by generating an apparent velocity weakening friction law that has been proposed empirically in earlier work. The analytical expression of the solution of the axial dynamics is used to derive an approximate analytical expression of the velocity weakening friction law related to the physical parameters of the system. This expression can be used to provide recommendations on the operating parameters and the drillstring or the bit design in order to reduce the amplitude of the torsional vibrations. Moreover, it is an appropriate candidate model to replace empirical friction laws encountered in torsional models used for control.

Key words. drillstring dynamics, discontinuous delay differential equations, stick-slip vibrations

AMS subject classifications. 34C15, 34C29, 34C60, 34D15, 37M99

DOI. 10.1137/060675848

1. Introduction.

Self-excited vibrations are phenomena commonly observed in rotary drilling systems used by oil industries. According to down-hole measurements [16], drilling systems permanently experience torsional vibrations, which often degenerate into stick-slip oscillations. These oscillations are characterized by stick phases, during which the rotation stops completely, and slip phases, during which the angular velocity of the tool increases up to two times the nominal angular velocity. Stick-slip oscillations are an important cause for drillstring failures and drag bit breakages. In order to reduce the costs of failures, considerable research effort has been dedicated in recent years to suppressing the large torsional vibrations. Diverse strategies, both active and passive, have been proposed in the literature to compensate for stick-slip vibrations; see [11, 13, 14, 19]. Control strategies usually operate at the ground surface by regulating the torque delivered to the drilling system or by adapting

*Received by the editors November 24, 2006; accepted for publication (in revised form) by J. Keener November 5, 2008; published electronically April 10, 2009. This work was supported by the Walloon Region and FSE agency (European Social Funding).
http://www.siam.org/journals/siads/8-2/67584.html
†Department of Electrical Engineering and Computer Science, University of Liege, BAT. B28 Systèmes et modélisation, Grande Traverse 10, B-4000 Liège, Belgium (christophe.germay@epslog.com, r.sepulchre@ulg.ac.be).
‡Mechanical Engineering, Dynamics and Control, University of Technology, P.O. Box 513, WH 0.131, 5600 MB Eindhoven, The Netherlands (n.v.d.wouw@tue.nl, h.nijmeijer@tue.nl).

the weight-on-bit.

Most of these studies rely on one- or two-degree-of-freedom (DOF) models that account for the torsional dynamics only. The oscillation mechanism arises from the friction model, which empirically captures the bit-rock interaction. The most common friction models include (i) velocity weakening laws as in [3, 4], (ii) stiction plus Coulomb friction (see [11, 19]), and (iii) models including the Stribeck effect (characterized by a decreasing friction-velocity map localized around zero velocity), with different degrees of complexity such as Karnop and LuGre models [5] that can be found in [12, 13, 14].

The diversity of these different friction models raises the question of the physical origin of the torsional vibrations. It complicates the synthesis of control laws designed to eliminate the oscillations in torsion and excludes the influence of the bit design on such vibrations.

In the present paper, we undertake the analysis of a new model, proposed in [17, 18], based on a physical and geometrical modeling of the bit-rock interaction. In this model, stick-slip vibrations do not result from an empirical friction model but rather from the dynamic coupling between the axial and torsional DOF of the drilling system.

In this approach, the axial vibrations are sustained by the regenerative effect associated with cutting. Namely, since the motion of the bit is helical, the thickness of the rock (or depth of cut) removed by a cutter at time t is affected both by its own axial position and by the path of the cutter ahead. As a consequence, the cutting force depends on the current axial position of the bit and a delayed axial position of the bit. This model is consistent with studies of chattering in metal machining [7, 10, 20, 22]. The regenerative effect is ultimately responsible for the coupling of the two modes of oscillations and for the existence of self-excited vibrations. A discontinuous term is present in the equations of motion due to the frictional contact taking place at the wearflat-rock interface.

Numerical simulations of this complicated system of equations exhibit stick-slip oscillations or bit bouncing phenomena for sets of parameters consistent with quantities measured in real field operations [17, 18]. Furthermore, an apparent bit-rock velocity weakening is recovered in the numerical simulations under certain conditions even though all the model parameters are rate-independent, including the friction coefficient. It has also been shown that a key parameter related to the bit shape has a dominant influence on the existence of stick-slip torsional vibrations.

A numerical analysis of the model is presented in [18]. It identifies the intermittent losses of the frictional contact at the wearflat-rock interface as the cause of the apparent decrease of the torque with the bit angular velocity. The losses of contact also contribute to a gain in drilling efficiency, as an energy transfer from the frictional contact to the pure cutting process occurs.

The complex and diversified numerical simulations in [18] motivate the analysis in the present paper aiming to identify the oscillation mechanisms and their parametric dependence. The proposed analysis exploits the presence of a large parameter in the axial governing equation leading to a two-time-scales separation between the fast axial dynamics and the slow torsional dynamics. The analysis uses a combination of averaging methods and a singular perturbation approach [21]. The study of the decoupled axial and torsional dynamics provides an explanation for the emergence of most of the different dynamic regimes observed in parameter space. We also derive an approximate analytical expression of the velocity weak-

ening law related to the physical parameters of the system. This expression can be used to provide recommendations on the operating parameters and the drillstring or the bit design in order to reduce the amplitude of the torsional vibrations. Moreover, it is an appropriate candidate to replace empirical friction laws encountered in torsional models used for control.

The paper is organized as follows. Section 2 is devoted to the derivation of the mathematical model of the drilling system and its main features. In section 3, we briefly present the methodology of analysis based on singular perturbation theory and the averaging method. The fast axial dynamics are analyzed in section 4. In section 5, an approximated analytical expression of the averaged axial dynamics is used in the analysis of the torsional dynamics. Section 6 shows some limitations of the two-time-scales approach. Finally, we draw some conclusions in section 7.

2. Drilling model.

2.1. Derivation of the dynamical model. A rotary drilling structure consists essentially of a rig, a drillstring, and a bit. The essential components of the drillstring are the bottom hole assembly (BHA), composed mainly of heavy steel tubes to provide a large downward force on the bit, and a set of drill pipes made of thinner tubes. For the idealized drilling system under consideration, we assume that the borehole is vertical and that there are no lateral motions of the bit.

The lumped parameter model of the drillstring presented in [17, 18], which is stripped to its essential elements, consists of an angular pendulum of stiffness C ended with a punctual inertia I and a punctual mass M free to move axially (see Figure 1) to represent the BHA and the bit as a unique rigid body. At the top of the drillstring, an upward force H_o and a constant angular velocity Ω_o are imposed. It is assumed that the weight-on-bit provided by the drillstring to the bit $W_o = W_s - H_o$ is constant, which implies that the hook load H_o is adjusted to compensate for the varying submerged weight of the drillstring W_s. The equations of motion of the drill bit and the BHA are then given by

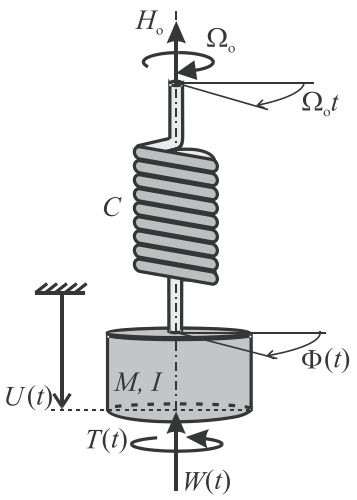

Figure 1. *Simplified model of a drilling system.*

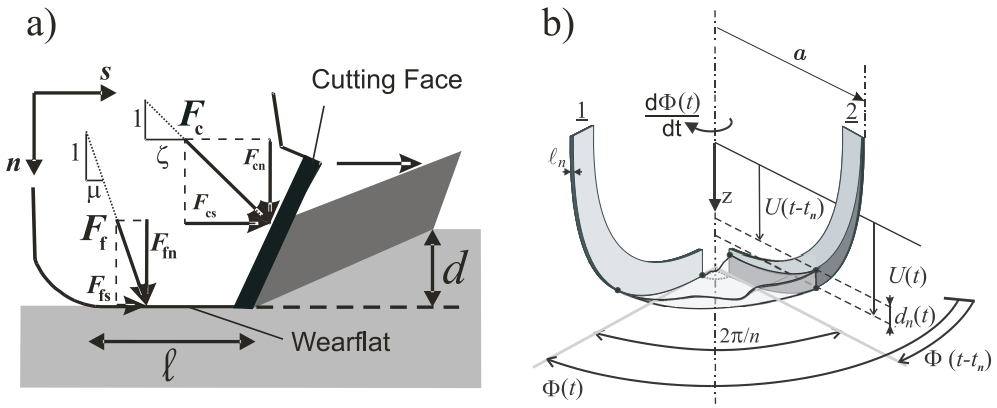

Figure 2. (a) *Sketch of forces acting on a single cutter;* (b) *section of the bottom-hole profile located between two successive blades of a drill bit (after* [18]*).*

$$I\frac{\mathrm{d}^2\Phi(t)}{\mathrm{d}t^2} + C\left(\Phi(t) - \Omega_{\mathrm{o}}t\right) = -T(t), \tag{2.1}$$

$$M\frac{\mathrm{d}^2U(t)}{\mathrm{d}t^2} = W_{\mathrm{o}} - W(t), \tag{2.2}$$

where U, Φ and t denote vertical, angular positions of the drag bit and time, respectively. The reacting torque-on-bit $T(t)$ and the reacting weight-on-bit $W(t)$ originate from the process of rock destruction occurring at the bit-rock interface.

The formulation of the bit-rock interface laws derives from a phenomenological model [6] of the forces acting on a single cutter of width w when removing rock over a constant depth d and constant longitudinal velocity, as sketched in Figure 2(a). The rock cutting consists of two independent processes: (i) a pure cutting process taking place at the cutting face (subscript $_{\mathrm{c}}$) and (ii) a frictional contact process (subscript $_{\mathrm{f}}$) along the interface between the wearflat of length ℓ (horizontal flat surface below the cutter) and the rock. The total force on the cutter is the sum of the cutting force $\mathbf{F}_{\mathrm{c}}$ and the friction force $\mathbf{F}_{\mathrm{f}}$, exerted on the cutting face and on the wearflat, respectively.

The vertical (subscript $_{\mathrm{n}}$) and horizontal (subscript $_{\mathrm{s}}$) components (see Figure 2(a)) of the cutting force and the friction force are expressed as

$$F_{\mathrm{cs}} = \varepsilon w d, \quad F_{\mathrm{cn}} = \zeta F_{\mathrm{cs}}, \quad F_{\mathrm{fs}} = \mu F_{\mathrm{fn}}, \quad F_{\mathrm{fn}} = \sigma w \ell,$$

where ε is the intrinsic specific energy (the minimum amount of energy required to destroy a unit volume of rock), ζ is a number characterizing the orientation of the cutting force, μ is the coefficient of friction, and σ is the maximum contact pressure at the wearflat-rock interface. When the wearflat is in conforming contact with the rock, σ is a constant parameter. Based on single cutter experiments, the value of this parameter can reasonably be assumed to be in the same range as ε [1, 2].

The distinction between cutting and friction forces is also relevant to modeling the generalized forces acting on a drill bit. The reacting torque-on-bit T and the reacting weight-on-bit W due to the operation of rock destruction account for both cutting and frictional processes,

$$T(t) = T_{\mathrm{c}}(t) + T_{\mathrm{f}}(t), \tag{2.3}$$

$$W(t) = W_{\mathrm{c}}(t) + W_{\mathrm{f}}(t). \tag{2.4}$$

The idealized drag bit of radius a consists of n identical radial blades regularly spaced by an angle of $2\pi/n$; see Figure 2(b). Each blade is characterized by a vertical cutting surface facing a depth of cut d_n and a wearflat of constant width ℓ_n orthogonal to the bit axis. The cumulative depth of cut of the bit is $d = nd_n$, and the equivalent wearflat width for the bit is $\ell = n\ell_n$.

By integrating the effects of all the individual cutters along the bit profile, the cutting components of W and T are given by [6]

$$W_{\mathrm{c}}(t) = na\zeta\varepsilon d_n(t), \quad T_{\mathrm{c}}(t) = n\frac{a^2}{2}\varepsilon d_n(t), \tag{2.5}$$

both proportional to the depth of cut $d_n(t)$ removed at time t. When the bit experiences vibrations, the rock ridge facing the blades varies. Because of the helicoidal motion (the bottom hole profile is dictated by the passage of the previous blade), the variable $d_n(t)$ is expressed by

$$d_n(t) = U(t) - U(t - t_n(t)), \tag{2.6}$$

where the delay t_n is the time required for the bit to rotate by an angle of $2\pi/n$. The delay t_n is the solution of the implicit equation

$$\int_{t-t_n(t)}^{t} \frac{\mathrm{d}\Phi(s)}{\mathrm{d}s}\mathrm{d}s = \Phi(t) - \Phi(t - t_n(t)) = \frac{2\pi}{n}. \tag{2.7}$$

A conceptual sketch is depicted in Figure 2(b).

The frictional components of W and T are given by

$$W_{\mathrm{f}} = na\ell_n\sigma\frac{(1 + \mathrm{sign}(\frac{\mathrm{d}U}{\mathrm{d}t}))}{2}, \quad T_{\mathrm{f}} = n\frac{a^2}{2}\gamma\mu\ell_n\sigma\frac{(1 + \mathrm{sign}(\frac{\mathrm{d}U}{\mathrm{d}t}))}{2}, \tag{2.8}$$

where the parameter γ depends on the spatial orientation and distribution of the wearflats along the bit profile [1]. The forces acting at the wearflat/rock are assumed constant once the wearflat is in conforming contact with the rock [18], i.e., when the bit moves downward $\frac{\mathrm{d}U}{\mathrm{d}t} > 0$. When the bit moves upward ($\frac{\mathrm{d}U}{\mathrm{d}t} < 0$), we assume a complete loss of contact between the wearflat and the rock, so that the frictional components W_{f} and T_{f} vanish. Note that referring to W_{f} as a frictional term is a slight abuse of language since it is a reaction force. Our terminology emphasizes that both T_{f} and W_{f} arise from the frictional process.

In the absence of vibrations, the nominal drilling solution ($\frac{\mathrm{d}U}{\mathrm{d}t} > 0$) is given by

$$\Phi_{\mathrm{o}} = \Omega_{\mathrm{o}}t - \frac{\left(T_{\mathrm{f}} + \frac{a(W_{\mathrm{o}} - W_{\mathrm{f}})}{2\zeta}\right)}{C}, \quad U_{\mathrm{o}}(t) = \frac{(W_{\mathrm{o}} - W_{\mathrm{f}})}{a\zeta\varepsilon}\frac{\Omega_{\mathrm{o}}}{2\pi}t, \tag{2.9}$$

where $T_{\mathrm{f}} + \frac{a(W_{\mathrm{o}} - W_{\mathrm{f}})}{2\zeta}$ is the nominal torque T_{o} and $(W_{\mathrm{o}} - W_{\mathrm{f}})/a\zeta\varepsilon$ is the nominal depth of cut.

The expression of the dimensionless equations that govern the bit motion, also referred to in the literature as the threshold-type delay equations, yields

$$\ddot{u}(\tau) = n\psi\left[-v_{\mathrm{o}}(\tau_n - \tau_{n\mathrm{o}}) - u(\tau) + u(\tau - \tau_n) + \lambda_n g(\dot{u}(\tau))\right], \tag{2.10}$$

$$\ddot{\varphi}(\tau) = n\left[-v_{\mathrm{o}}(\tau_n - \tau_{n\mathrm{o}}) - u(\tau) + u(\tau - \tau_n) + \beta\lambda_n g(\dot{u}(\tau))\right] - \varphi(\tau), \tag{2.11}$$

$$\int_{\tau-\tau_n(\tau)}^{\tau} (\omega_{\mathrm{o}} + \dot{\varphi}(s))\,\mathrm{d}s = \frac{2\pi}{n}, \tag{2.12}$$

where $u(\tau) = (U - U_{\mathrm{o}})/L_*$ and $\varphi(\tau) = \Phi - \Phi_{\mathrm{o}}$ represent the dimensionless axial and angular deviation to the nominal solutions, respectively. The dot denotes differentiation with respect to the dimensionless time $\tau = t/\sqrt{I/C}$. The characteristic length is given by $L_* = 2C/\varepsilon a^2$. In the absence of torsional vibrations, $\varphi = 0$ and $\tau_n = \tau_{n\mathrm{o}} = 2\pi/n\omega_{\mathrm{o}}$; in the absence of axial vibrations, $u = u(\tau - \tau_n) = 0$. The function $g(\dot{u})$ in (2.10) is defined as

$$g(\dot{u}) = \frac{1}{2}\left(1 - \mathrm{Sign}(\dot{u} + v_{\mathrm{o}})\right). \tag{2.13}$$

Physically, the dimensionless normalized term $g(\dot{u})$ is the complement of the normalized reacting force $W_{\mathrm{f}}/na\ell_n\sigma$, i.e., $g(\dot{u}) + W_{\mathrm{f}}/na\ell_n\sigma = 1$.

The dimensionless parameters of the model (2.10)–(2.12) are the following:

(i) the control parameters $\mathcal{W}_{\mathrm{o}} = aW_{\mathrm{o}}/2\zeta C$ and $\omega_{\mathrm{o}} = \Omega_{\mathrm{o}}\sqrt{I/C}$;
(ii) the nominal dimensionless reacting force $\lambda = n\lambda_n = na^2\ell_n\sigma/2\zeta C$ is proportional to the length of the wears (it is an image of the bluntness of the bit);
(iii) the nominal axial bit velocity $v_{\mathrm{o}} = \omega_{\mathrm{o}}(\mathcal{W}_{\mathrm{o}} - \lambda)/2\pi$;
(iv) the lumped parameter $\beta = \mu\gamma\zeta$ characterizes the geometry of the bit;
(v) the lumped parameter $\psi = \zeta\varepsilon aI/MC$ characterizes the drill string design.

The set of equations (2.10)–(2.12) is nonlinear, coupled, and contains a state-dependent delay. Furthermore, the frictional process causes a discontinuous term $g(\dot{u})$ in (2.10) and (2.11). The solutions of the discontinuous differential equation are defined in Filippov's sense. Filippov's convex method [8] treats the discontinuous function $g(\dot{u})$ as a convex set-valued mapping on the hyperplane $\dot{u} = -v_{\mathrm{o}}$; i.e., $\mathrm{Sign}(x)$ maps 0 to the set $[-1, 1]$.

2.2. Stick modeling.

2.2.1. Axial stick.

- A stick phase may occur in the axial dynamics, only when the axial vibrations cause the axial velocity $\dot{U}$ to become zero for a limited period of time although the bit is still rotating forward $\left(\dot{\Phi} > 0\right) \equiv (\dot{\varphi}(\tau) > -\omega_{\mathrm{o}})$. We refer to this situation as the *axial stick* phase during which the axial position of the bit is stationary ($U = const$). It corresponds to the situation where the applied weight-on-bit W_{o} can be compensated by the cutting force W_{c} and a portion of the reacting force W_{f}. In dimensionless form, the latter is upperbounded by λ, and the mathematical conditions for an axial stick phase are as follows:

$$0 \in n\psi\left[-v_{\mathrm{o}}(\tau_n - \tau_{n\mathrm{o}}) - u(\tau) + u(\tau - \tau_n) + \frac{\lambda_n}{2}\left(1 - \mathrm{Sign}(0)\right)\right] \tag{2.14}$$

$$\Rightarrow \left[-v_{\mathrm{o}}(\tau_n - \tau_{n\mathrm{o}}) - u(\tau) + u(\tau - \tau_n) + \frac{\lambda_n}{2}\right]\frac{2}{\lambda_n} \in [-1, 1]. \tag{2.15}$$

The value of $g(\dot{u})$ during the axial stick phase is given by

$$g(\dot{u} = -v_o) = \frac{v_o(\tau_n - \tau_{no}) + u(\tau) - u(\tau - \tau_n)}{\lambda_n}. \tag{2.16}$$

2.2.2. Torsional stick. The torsional model (2.11) is valid as long as $\dot{\varphi} > -\omega_o$, which corresponds to a *slip* phase. The torsional vibrations may become so severe that the sign of the velocity is reversed. In this case, the magnitude of the frictional torque is assumed to be sufficient to restrain the bit from rotating backward. The system then enters a *stick* phase during which the bit sticks to the rock. The torsional *stick* phase is modeled by

$$\left(\dot{\Phi} = 0\right) \equiv \left(\dot{\varphi}(\tau) = -\omega_o\right), \tag{2.17}$$

$$\left(\dot{U} = 0\right) \equiv \left(\dot{u} = -v_o\right). \tag{2.18}$$

The stick equations (2.17)–(2.18) are substituted into (2.10) and (2.11) until the right-hand side of (2.11) becomes positive and the bit enters a new slip phase. Physically, since the rotation of the drill pipes continues at the surface, the torque applied by the drillstring onto the BHA builds up until its magnitude is sufficient to overcome the reacting torque, causing the bit to rotate.

2.3. Bit bouncing. Model (2.10)–(2.12) loses its validity when the dimensionless depth of cut

$$\delta = n\left[v_o\tau_n + (u(\tau) - u(\tau - \tau_n))\right] \tag{2.19}$$

becomes negative. This event will be referred to as *bit bouncing*, which is detrimental for the bit. It occurs when the bit experiences sufficiently large axial vibrations to disengage completely from the rock formation. The objective of the design is to avoid it.

3. Two-time-scales analysis. In view of the complexity of the model, its mathematical analysis is not straightforward. However, two clearly distinct time scales (see Figure 11) emerge due to the magnitude of the parameter ψ, which is typically of order 10^2–10^3. In the remainder of the paper, we consider the model (2.10)–(2.12) in the singularly perturbed form

$$\epsilon^2\ddot{u}(\tau) = -\left[v_o(\tau_n - \tau_{no}) + u(\tau) - u(\tau - \tau_n) - \lambda_n g(\dot{u}(\tau))\right], \tag{3.1}$$

$$\ddot{\varphi}(\tau) + \varphi(\tau) = -n\left[(1-\beta)\lambda_n g(\dot{u}(\tau)) - \epsilon^2\ddot{u}(\tau)\right], \tag{3.2}$$

$$\int_{\tau-\tau_n(\tau)}^{\tau} (\omega_o + \dot{\varphi}(t))\,\mathrm{d}t = \frac{2\pi}{n}, \tag{3.3}$$

where $1/\sqrt{n\psi} = \epsilon > 0$ is a small parameter. In this configuration, the axial dynamics will be considered as "fast" dynamics, and the torsional dynamics as "slow" dynamics. Indeed, the characteristic dimensionless time of the torsional oscillations is $\tau_t \approx 2\pi$, while the characteristic dimensionless time of the axial oscillations is $\tau_a \approx 2\pi/\sqrt{\psi}$.

In the classical singular perturbation theory, the fast system can be studied independently by freezing the slow variables. Commonly called the boundary layer system, it consists of

trajectories that converge exponentially to a slow manifold. Upon convergence of the boundary layer, solutions evolve on the so-called reduced model that provides a good estimate of the slow dynamics.

In the particular system (3.1)–(3.3), solutions of the boundary layer converge towards a family of limit cycles that depends on the parameters of the system. Nonetheless, the authors of [21] provide a unification framework that combines averaging methods and singular perturbation approach to handle systems with complex fast dynamics. Although the theory has not been fully developed for our particular type of equation (threshold type with discontinuous terms), we adopt a similar approach to analyze the dynamics of the complete system (3.1)–(3.3).

In the next section, the fast axial dynamics of (3.1) are studied under the simplifying assumption that the delay τ_n is a fixed parameter. Under certain conditions, numerical simulations show that stable oscillations in $\dot{u}$ are observed. We will propose an analytical approximation of the fast axial solution. In section 5, this approximation will be used to study the slow torsional dynamics by means of averaging methods.

4. Axial dynamics. In order to observe the periodic oscillations in $\dot{u}$ as a true limit cycle, a proper coordinate transformation is in place, where the new set of state variables must be of zero derivative mean over the limit cycle. Let us assume that periodic oscillations exist in $\dot{u}$. Then, we may write that

$$\langle \ddot{u}(\tau) \rangle_a = \frac{1}{\tau_a} \int_{\tau-\tau_a/2}^{\tau+\tau_a/2} \ddot{u}\,(s)\,\mathrm{d}s = 0. \tag{4.1}$$

In the simplest case where $\tau_n = \tau_{no}$, which is not contradictory with the existence of an axial limit cycle as will be shown below, the equality

$$\langle u(\tau) - u\,(\tau - \tau_n) \rangle_a = \lambda_n \langle g(\dot{u}\,(\tau)) \rangle_a \tag{4.2}$$

is obtained by averaging (3.1) with (4.1) over one axial limit cycle, where the mean value of the only nonlinear term $\langle g(\dot{u}\,(\tau)) \rangle_a$ in (3.1) is nonzero. Therefore, a drift of the solution in the u-direction with a velocity depending on $\lambda_n \langle g(\dot{u}\,(\tau)) \rangle_a$ exists. Note that $\langle g(\dot{u}\,(\tau)) \rangle_a$ is a priori unknown as it is a function of $\dot{u}\,(\tau)$; i.e., it depends on the solution of (3.1).

For this reason, we introduce a new set of state variables of zero derivative mean over an axial limit cycle

$$\begin{aligned} w_1\,(\bar{\tau}) &= u\,(\bar{\tau} - \bar{\tau}_n) - u\,(\bar{\tau}) - \bar{v}_o\,(\bar{\tau}_n - \bar{\tau}_{no})\,, \\ w_2\,(\bar{\tau}) &= \dot{u}\,(\bar{\tau})\,/\sqrt{n\psi}, \end{aligned}$$

that evolves in the fast time scale $\bar{\tau} = \tau\sqrt{n\psi}$ and where $\bar{v}_o = v_o/\sqrt{n\psi}$, $\bar{\tau}_n = \tau_n\sqrt{n\psi}$, and $\bar{\tau}_{no} = \tau_{no}\sqrt{n\psi}$. Physically, the new variable w_1 represents the negative discrepancy between the dimensionless form of the depth of cut and the nominal one. In the new variables, the axial equation (3.1) admits the state-space representation

$$\mathring{w}_1\,(\bar{\tau}) = w_2\,(\bar{\tau} - \bar{\tau}_n) - w_2\,(\bar{\tau})\,, \tag{4.3}$$

$$\mathring{w}_2\,(\bar{\tau}) = w_1\,(\bar{\tau}) + \lambda_n \bar{g}(w_2\,(\bar{\tau})), \tag{4.4}$$

with

$$\bar{g}(w_2) = \frac{1}{2}\left(1 - \operatorname{sign}\left(w_2 + \bar{v}_{\mathrm{o}}\right)\right). \tag{4.5}$$

The limit cycle observed in the new state (w_1, w_2) space will be understood as the axial limit cycle. The system (4.3)–(4.4) is referred to as the fast system. The round dot denotes differentiation with respect to the stretched time $\bar{\tau}$. The initial condition required to solve the infinite dimensional axial dynamics (3.1) is the function $u(\cdot)$ on the time interval $[-\tau_n, 0]$. In the new variables, this initial condition translates into the function $w_2(\cdot)$ on the time interval $[-\bar{\tau}_n, 0]$ and

$$w_1(0) = -\bar{v}_{\mathrm{o}}\left(\bar{\tau}_n - \bar{\tau}_{n\mathrm{o}}\right) - \int_{-\bar{\tau}_n}^{0} w_2(t)\mathrm{d}t. \tag{4.6}$$

The equilibrium solution of (4.3)–(4.4) with (4.6) is $(w_1, w_2) = (0, -\bar{v}_{\mathrm{o}}\left(\bar{\tau}_n - \bar{\tau}_{n\mathrm{o}}\right)/\bar{\tau}_n)$. Physically, it corresponds to the rigid translation $\dot{u} = -v_{\mathrm{o}}\left(\tau_n - \tau_{n\mathrm{o}}\right)/\tau_n$, $u\left(\tau - \tau_n\right) - u\left(\tau\right) = v_{\mathrm{o}}\left(\tau_n - \tau_{n\mathrm{o}}\right)$.

In a neighborhood of this equilibrium, the reacting force W_{f} at the wearflat-rock interface is permanent $(w_2 > -\bar{v}_{\mathrm{o}})$, as its dimensionless complement $\bar{g}(w_2)$ is 0. The dynamics $\mathring{w}_1\left(\bar{\tau}\right) = w_2\left(\bar{\tau} - \bar{\tau}_n\right) - w_2\left(\bar{\tau}\right)$ and $\mathring{w}_2\left(\bar{\tau}\right) = w_1\left(\bar{\tau}\right)$ are then linear. Stability of the equilibrium is thus determined by the location of the roots of the characteristic function

$$P(s) = s^2 + 1 - e^{-s\bar{\tau}_n}. \tag{4.7}$$

This function does not have roots in the right half of the complex plane when $\bar{\tau}_n < \pi/\sqrt{2}$. Two complex conjugated roots pass from the left half-plane to the right half-plane at the critical value $\bar{\tau}_n = \pi/\sqrt{2}$. They remain in the open right half-plane for $\bar{\tau}_n > \pi/\sqrt{2}$. Consequently, the equilibrium point $(w_1, w_2) = (0, -\bar{v}_{\mathrm{o}}\left(\bar{\tau}_n - \bar{\tau}_{n\mathrm{o}}\right)/\bar{\tau}_n)$ is exponentially stable when $\bar{\tau}_n < \pi/\sqrt{2}$, marginally stable when $\bar{\tau}_n = \pi/\sqrt{2}$, and unstable when $\bar{\tau}_n > \pi/\sqrt{2}$. In typical field operations, the delay satisfies $\bar{\tau}_n > \pi/\sqrt{2}$, meaning that the equilibrium solution is unstable.

The growth of the solutions of (4.3)–(4.4) away from this unstable equilibrium is limited by the nonlinear friction. Under certain conditions, this mechanism is responsible for the existence of an axial stick-slip limit cycle. The next section provides a qualitative description of this limit cycle in the phase plane (w_1, w_2).

4.1. Analysis of the axial limit cycle. When the equilibrium of (4.3)–(4.4) is unstable $(\bar{\tau}_n > \pi/\sqrt{2})$, numerical simulations indicate that the solutions of (4.3)–(4.4) either grow unbounded (ultimately leading to bit bouncing as described in section 2.3) or converge to a limit cycle that fits the qualitative description of Figure 3.

In the state space (w_1, w_2), the axial limit cycle illustrated in Figure 3 can be decomposed into three different phases: a slip phase, a stick phase, and a sliding phase. By choosing arbitrarily the origin of time as $w_1(0) = 0$, $w_2(0) = -v_{\mathrm{o}}$, and $\mathring{w}_1(0) > 0$, the temporal sequence of these three phases during one period $[0, \bar{\tau}_a]$ of the cycle is as follows:

(i) The slip phase $(\bar{\tau} \in [0, \bar{\tau}_k])$ is characterized by the condition $w_2\left(\bar{\tau}\right) > -v_{\mathrm{o}}$. As a consequence, $\bar{g}(w_2) = 0$, and the solution obeys the unstable linear dynamics

$$\mathring{w}_1\left(\bar{\tau}\right) = w_2\left(\bar{\tau} - \bar{\tau}_n\right) - w_2\left(\bar{\tau}\right), \tag{4.8}$$

$$\mathring{w}_2\left(\bar{\tau}\right) = w_1\left(\bar{\tau}\right). \tag{4.9}$$

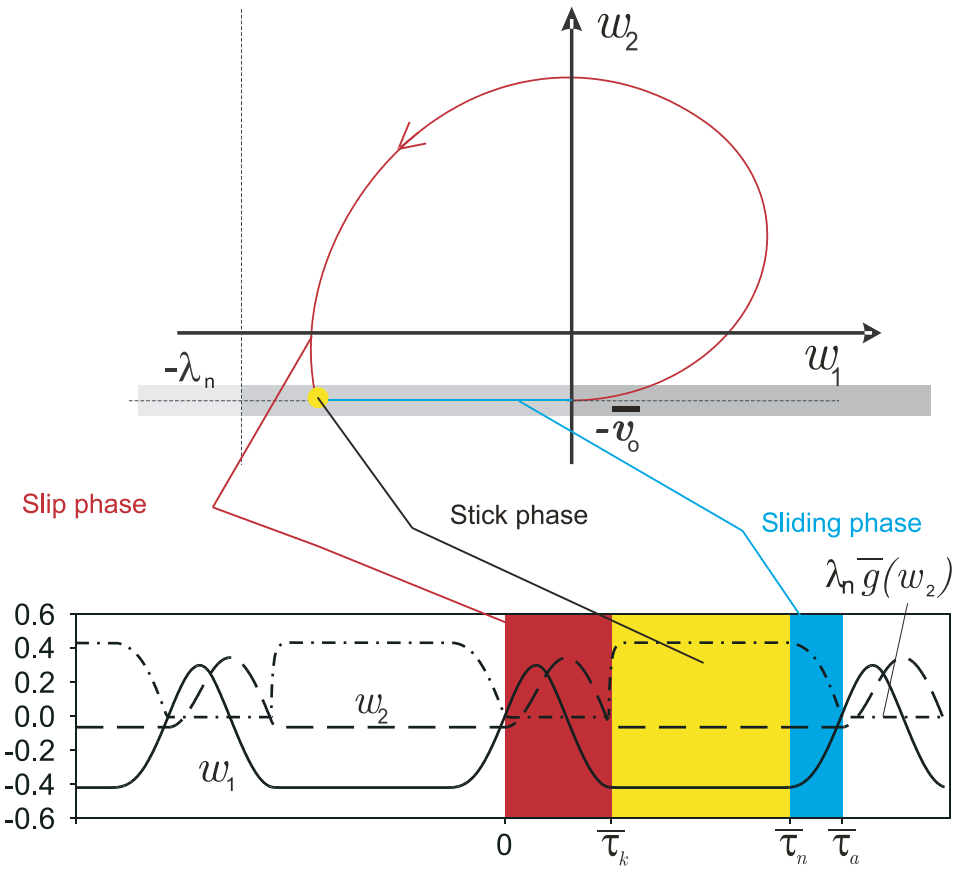

Figure 3. *Axial limit cycle in the space* (w_1, w_2) *and the corresponding evolution of* w_1, w_2, *and* $\lambda_n \bar{g}(w_2)$ *in time.*

During this phase, $w_2(\bar{\tau} - \bar{\tau}_n)$ is initially greater than $-v_o$ (due to the previous slip phase) and larger than $w_2(\bar{\tau})$; i.e., $w_1(\bar{\tau})$ and $w_2(\bar{\tau})$ increase according to (4.8) and (4.9), respectively. When $w_2(\bar{\tau})$ becomes larger than $w_2(\bar{\tau} - \bar{\tau}_n)$, $w_1(\bar{\tau})$ decreases and becomes negative, causing $w_2(\bar{\tau})$ to decrease. During that lapse of time, $w_2(\bar{\tau} - \bar{\tau}_n)$ has reached the previous stick phase ($w_2(\bar{\tau} - \bar{\tau}_n) = -v_o$). When $w_2(\bar{\tau})$ becomes equal to $-v_o$, the system enters the stick phase.

(ii) The stick phase ($\bar{\tau} \in [\bar{\tau}_k, \bar{\tau}_n]$) is characterized by constant axial velocity $w_2 = -\bar{v}_o$ and constant friction $\lambda_n \bar{g}(w_2) = -w_1(\bar{\tau}_k)$. The projection of the solution in the phase plane (w_1, w_2) has shrunk to one point. This phase will last until the delayed solution $w_2(\bar{\tau} - \bar{\tau}_n)$ enters a slip phase described in (i). It happens when $\bar{\tau} = \bar{\tau}_n$. Note that the existence of the stick phase, necessary to observe the axial stick-slip limit cycle, relies on the conditions $0 \leq -w_1(\bar{\tau}_k) \leq \lambda_n$ and $\bar{\tau}_k \leq \bar{\tau}_n$.

(iii) During the sliding phase ($\bar{\tau} \in [\bar{\tau}_n, \bar{\tau}_a]$), the axial velocity is still at rest ($w_2(\bar{\tau}) = -\bar{v}_o$), but the delayed axial velocity $w_2(\bar{\tau} - \bar{\tau}_n) > -\bar{v}_o$ when $\bar{\tau} > \bar{\tau}_n$, causing $w_1(\bar{\tau})$ to slide along the line $w_2(\bar{\tau}) = -\bar{v}_o$ in the state space (w_1, w_2). The term $\lambda_n \bar{g}(w_2(\bar{\tau}))$ decreases accordingly until it reaches 0, i.e., the minimum value that $\bar{g}(w_2(\bar{\tau}))$ can

attain. Then a new cycle starts.

The reader should note that the stick phase defined in section 2.2.1 (U and $\dot{U}$ constant) consists of the stick phase (w_1 and w_2 constant) *and* the sliding phase ($w_2 = -\bar{v}_o$ and $\dot{w}_1 > 0$) in the new variables. Numerical simulations show also the existence of the axial limit cycle when $-w_1(\bar{\tau}_k)$ is slightly greater than λ_n. The trajectories pass below the line $w_2 = -\bar{v}_o$ and stick onto $w_2 = -\bar{v}_o$ somewhat later. We do not consider this case here since it arises in a very small region of the set of parameters.

In the next section, we derive an approximate solution for this limit cycle that allows for an analytic prediction of the influence of key system parameters on this limit cycle. These analytical predictions are compared to numerical solutions obtained from solving the fast dynamics by a shooting method [15].

4.2. Analytical approximation of the axial limit cycle.

Slip phase: To approximate the time evolution of the limit-cycle solution shown in Figure 3, we assume that the delayed axial velocity is zero ($w_2(\bar{\tau} - \bar{\tau}_n) = -\bar{v}_o$) during the slip phase $\bar{\tau} \in [0, \bar{\tau}_k]$. The resulting linear system

$$\mathring{w}_1 = -\bar{v}_o - w_2, \tag{4.10}$$

$$\mathring{w}_2 = w_1, \tag{4.11}$$

is solved for the initial condition $w_2(0) = -\bar{v}_o$, which yields

$$w_1(\bar{\tau}) = C_1 \cos\bar{\tau}, \tag{4.12}$$

$$w_2(\bar{\tau}) = C_1 \sin\bar{\tau} - \bar{v}_o, \quad \bar{\tau} \in [0, \bar{\tau}_k]. \tag{4.13}$$

Stick phase: The approximated solution (4.12)–(4.13) enters the stick phase at $\bar{\tau}_k = \pi$ when $w_2(\bar{\tau}_k)$ becomes equal to $-\bar{v}_o$. The dimensionless term $\lambda_n \bar{g}(w_2)$ associated with the frictional process increases suddenly ($\lambda_n \bar{g}(w_2) = -w_1(\bar{\tau}_k) = C_1$ according to (4.12)) such that $\mathring{w}_2(\bar{\tau}) = 0$ during the stick phase. The necessary condition for observing a stick phase is $w_2(\bar{\tau} - \bar{\tau}_n) = w_2(\bar{\tau}) = -\bar{v}_o \Rightarrow \bar{\tau}_n > \pi$, which satisfies the condition of instability of the axial equilibrium ($\bar{\tau}_n > \pi/\sqrt{2}$), and $-w_1(\bar{\tau}_k) \leq \lambda_n$.

Sliding phase: The solution in the sliding phase is given by

$$w_1(\bar{\tau}) = -C_1 \cos(\bar{\tau} - \bar{\tau}_n), \tag{4.14}$$

$$w_2(\bar{\tau}) = -\bar{v}_o. \tag{4.15}$$

The (approximate) solution returns to the initial state when $w_1(\bar{\tau}) = C_1$, i.e., at time $\bar{\tau}_a = \pi + \bar{\tau}_n$.

The free constant C_1 in (4.12)–(4.13) is determined from the initial condition

$$w_1(0) = C_1 = \bar{v}_o \bar{\tau}_{no} - \int_{-\bar{\tau}_n}^{0} w_2(t) + \bar{v}_o \mathrm{d}t.$$

Since $w_2(\bar{\tau}) = -\bar{v}_o$ over $[-\bar{\tau}_n, 0]$, we obtain

$$C_1 = \bar{v}_o \bar{\tau}_{no}, \tag{4.16}$$

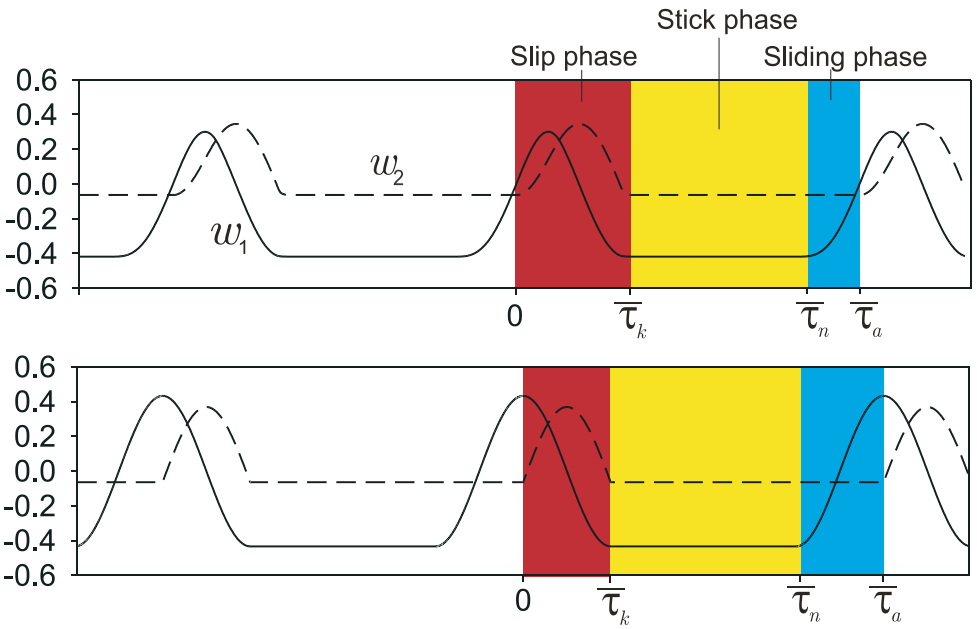

Figure 4. *Top: Limit cycle of w_1 and w_2 with $\bar{\tau}$. Bottom: Approximated limit cycle of w_1 and w_2 in terms of $\bar{\tau}$.*

which corresponds to the nominal depth of cut per blade. The time evolution of the axial limit cycle solution and its approximation are illustrated in Figure 4.

The approximate solution of the limit cycle provides the following predictions:

- The period of the limit cycle is estimated as $\bar{\tau}_a = \pi + \bar{\tau}_n$. It grows linearly with the delay and is independent of the parameters $\bar{v}_o$ and $\bar{\tau}_{no}$.
- The amplitude of the limit cycle is estimated as $C_1 = \bar{v}_o \bar{\tau}_{no}$, regardless of the delay $\bar{\tau}_n$. It must be less than λ_n to observe a stick phase, which is essential to the existence of the axial limit cycle, as otherwise bit bouncing will eventually take place.
- In the next section, we will see that the axial dynamics influence the torsional dynamics through the average value of $\bar{g}(w_2(\bar{\tau}))$ over one axial limit cycle. By using (2.16) with (4.5), $\lambda_n \bar{g}(w_2(\bar{\tau}))$ is different from zero only during the stick and the sliding phase where it takes the value $-w_1(\bar{\tau})$. Figure 4 illustrates that $-w_1(\bar{\tau})$ takes both positive and negative values over one period of the approximate limit cycle, which is in contrast to the (physical meaningful) property that $\bar{g}$ should take only positive values in the exact model. To correct for this artifact, we compute the averaged frictional term $\lambda_n \langle \bar{g}(w_2(\bar{\tau})) \rangle_a$ using the approximate limit cycle, but we restrict the interval of integration to the positive values of $\bar{g}(w_2(\bar{\tau}))$ only, i.e., on the time-interval $[0, \bar{\tau}_n + \pi/2]$, yielding

$$\lambda_n \langle \bar{g}(w_2(\bar{\tau})) \rangle_a = \frac{1}{\bar{\tau}_a} \int_0^{\bar{\tau}_a} \lambda_n \bar{g}(w_2(s)) \mathrm{d}s \tag{4.17}$$

$$\approx -\frac{1}{\bar{\tau}_n + \pi} \int_{\pi}^{\bar{\tau}_n + \pi/2} w_1(s)\, \mathrm{d}s = \frac{\bar{v}_o \bar{\tau}_{no} (\bar{\tau}_n - \pi + 1)}{(\bar{\tau}_n + \pi)}. \tag{4.18}$$

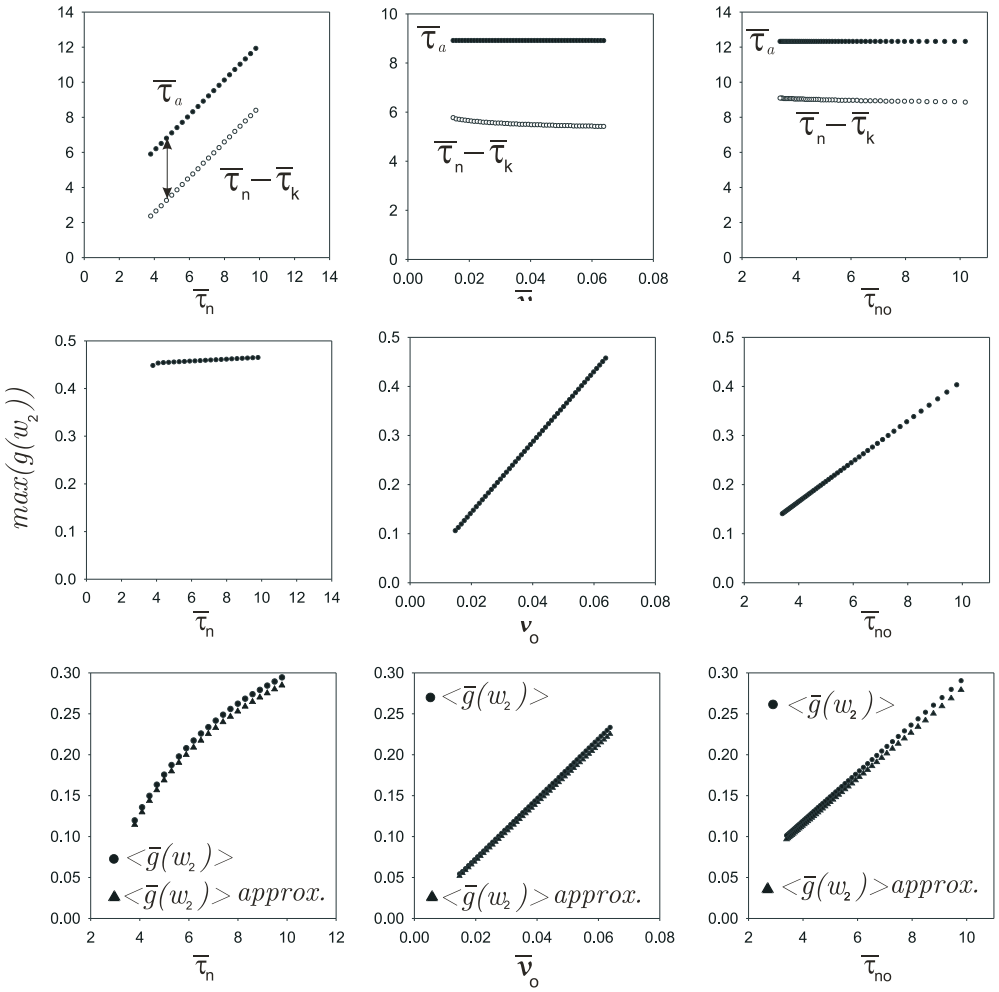

Figure 5. *Top: Period of the axial limit cycle for different values of $\bar{\tau}_n$, $\bar{v}_o$, and $\bar{\tau}_{no}$. Middle: Maximum values of $\bar{g}(w_2)$ with respect to $\bar{\tau}_n$ ($\bar{v}_o = 0.063$, $\bar{\tau}_{no} = 6.8$), $\bar{v}_o$ ($\bar{\tau}_n = 6.8$, $\bar{\tau}_{no} = 5.8$), and $\bar{\tau}_{no}$ ($\bar{v}_o = 0.043$, $\bar{\tau}_{no} = 10.18$), respectively (these results are obtained by solving the fast system with the shooting method). Bottom: Comparison between the results obtained with the approximative and the fast systems.*

It is linear in the parameters $\bar{v}_o$ and $\bar{\tau}_{no}$. It is a monotonic function of the delay, but its dependency saturates as the delay increases. Note that $\langle \bar{g}(w_2(\bar{\tau})) \rangle_a$ becomes zero when $\bar{\tau}_n = \pi - 1$, which almost agrees with the condition of stability of the axial equilibrium $\pi/\sqrt{2}$.

Figure 5 illustrates the excellent match between these analytical predictions and the numerical results obtained from a shooting method applied to the exact model.

We see that $\bar{\tau}_n$ does not affect the amplitude of the periodic orbit but varies linearly with $\bar{v}_o$ and $\bar{\tau}_{no}$ as predicted by the approximated system. The period of the orbit is influenced only by $\bar{\tau}_n$, and the average value is an excellent approximation of the solutions obtained from the full model.

When the bit angular velocity is small, the delay is large, and the system spends most of the time in the stick phase where the frictional contact force between the wearflat and the rock is constant. This corresponds in Figure 5 to the increase of $\lambda_n \langle \bar{g}(w_2(\bar{\tau})) \rangle_a$ with $\bar{\tau}_n$.

4.3. Bit bouncing. Bit bouncing occurs when both the equilibrium solution and the limit cycle solution of the axial dynamics are unstable. The amplitude of the vibrations grows exponentially, and the bit ultimately loses contact with the rock completely.

The existence of the axial limit cycle discussed in the previous section requires the condition

$$0 \leq -w_1(\bar{\tau}_k) \leq \lambda_n. \tag{4.19}$$

We use condition (4.19) together with the parametric condition $\bar{\tau}_n > \pi/\sqrt{2}$ (which guarantees that the equilibrium is unstable) as a prediction of the parametric range in which a stable axial limit cycle exists.

Because $-w_1(\bar{\tau}_k) = \bar{v}_o \bar{\tau}_{no}$ in the approximation (4.12)–(4.16), equation (4.19) translates into the parametric condition $\bar{v}_o \bar{\tau}_{no} < \lambda_n$, which, rewritten in the original parameters of the model, is equivalent to the condition

$$\mathcal{W}_o/\lambda < 2, \tag{4.20}$$

where we recall that $\mathcal{W}_o$ is related to the applied weight-on-bit and λ is proportional to the length of the wears (bluntness of the bit).

This prediction is in good agreement with the stability map in Figure 6, numerically computed from the full model (2.10)–(2.12), as shown in [9]. To draw the map, we simulated 300 bit revolutions for each pair of values $(\mathcal{W}_o, \lambda)$. If the depth of cut becomes negative, the computation is stopped and the corresponding value $(\mathcal{W}_o, \lambda)$ is given the dark grey color; otherwise a light grey color is chosen. The black region indicates parameter values for which the bit is not drilling but is only in frictional contact. In that case, the dimensionless applied weight-on-bit $\mathcal{W}_o$ does not overcome the nominal dimensionless frictional term λ (i.e., the weight-on-bit transmitted by the wearflats when the bit is drilling). In the absence of torsional vibrations, i.e., when $\dot{\varphi} = 0$, the theoretical analysis predicts no bit bouncing when the axial equilibrium is stable ($\bar{\tau}_{no} = \bar{\tau}_n < \pi/\sqrt{2} \Leftrightarrow \omega_o > \omega_o^s = 2\sqrt{2\psi/n}$) or when $\mathcal{W}_o/\lambda < 2$. These predictions are mainly illustrated in Figure 7, although the numerical results are obtained from the complete system (2.10)–(2.12) where the bit experiences torsional vibrations. The three different axial regimes (stable equilibrium, stable limit cycle, bit bouncing) are represented in the parametric plane $(\omega_o, \mathcal{W}_o)$. We conclude that the predictions of the analytical approximation of the axial limit cycle are accurate in detecting the transitions, such as stability of the axial equilibrium, stability of the axial limit cycle, and bit bouncing.

5. Torsional dynamics. The reduced (slow) dynamics governing the torsional motion is obtained by assuming the following:

1. The slow variables are constant over the period of oscillations of the axial vibrations:

$$\langle f(\tau) \rangle_a = \frac{1}{\tau_a} \int_{\tau - \tau_a/2}^{\tau + \tau_a/2} f(\tau + s)\, \mathrm{d}s \approx f(\tau), \tag{5.1}$$

where f can be either φ, $\dot{\varphi}$, $\ddot{\varphi}$ or τ_n and $\tau_a = \bar{\tau}_a/\sqrt{n\psi}$.

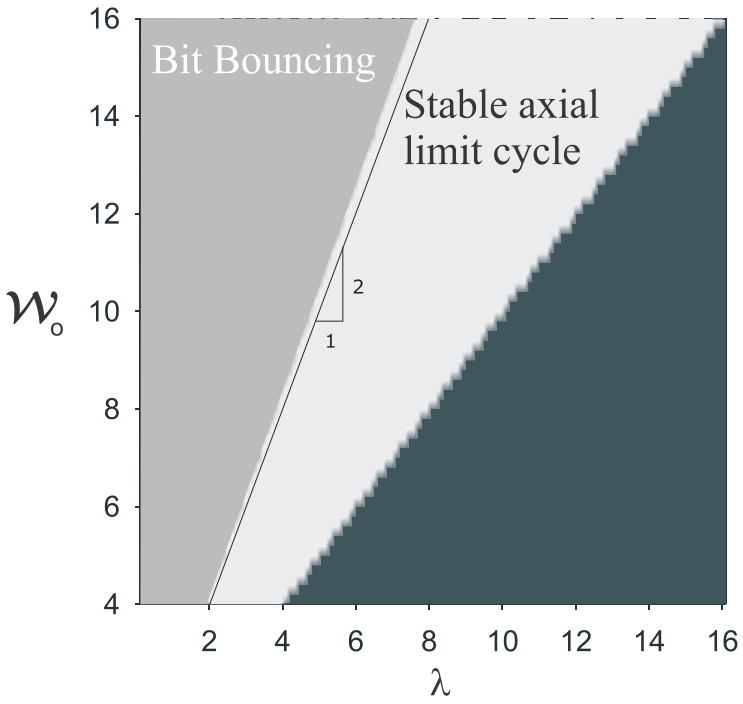

Figure 6. *Map of stability for values of* $(\mathcal{W}_o, \lambda)$ *(*$n = 6$*,* $\beta = 0.276$*,* $\omega_o = 4$*,* $\psi = 63.1$*); after* [9].

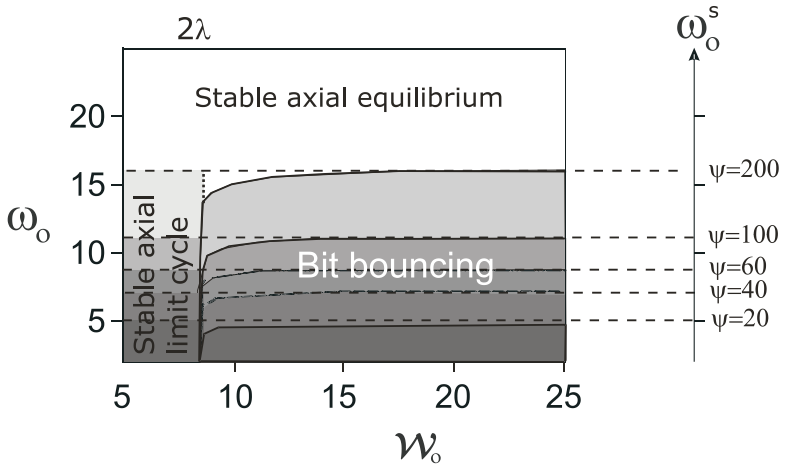

Figure 7. *Numerical map of stability for different rotational speeds* ω_o *and* ψ *when* $n = 6$*,* $\beta = 0.43$*, and* $\lambda = 4.2$*; after* [18].

2. The mean axial acceleration along a periodic solution of the axial limit cycle is zero:

$$\langle \ddot{u}\,(\tau, \tau_n)\rangle_a = 0. \tag{5.2}$$

By averaging (3.2) over a period of the axial limit cycle $\tau_a(\tau_n)$, the reduced model yields

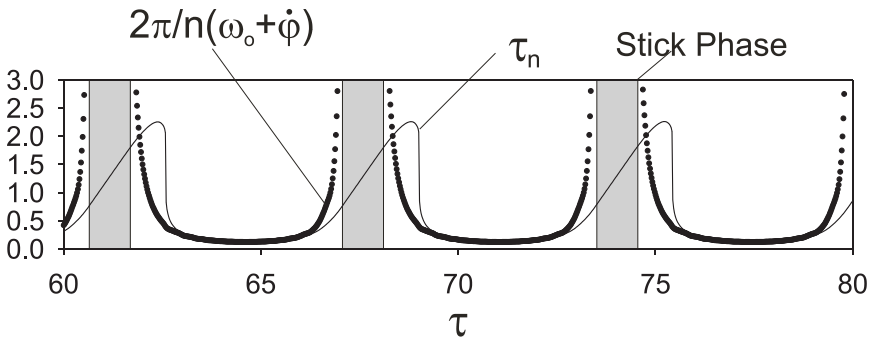

Figure 8. *Comparison between the real delay τ_n and the approximation $\frac{2\pi}{n(\omega_o+\dot{\varphi})}$ during three stick-slip cycles.*

$$\ddot{\varphi}(\tau) + \varphi(\tau) = -n(1-\beta)\lambda_n \langle g(\dot{u}(\tau, \tau_n))\rangle_a . \tag{5.3}$$

Together with (3.3), this equation forms the reduced system.

5.1. Analytical approximation of the torsional dynamics. To facilitate the analysis of the slow dynamics, we derive an explicit relationship linking $\tau_n(\tau)$ and the bit angular velocity $\dot{\varphi}(\tau)$. Most of the time, the delay τ_n is of the order of 10^{-1}, which is small compared to the characteristic time 2π of the torsional oscillations. For this reason, we treat the torsional variable $\dot{\varphi}(\tau)$ as a constant over the delay $\tau_n(\tau)$, and its expression yields

$$\int_{\tau-\tau_n(\tau)}^{\tau} (\omega_o + \dot{\varphi}(t))\,dt \approx \tau_n(\tau)(\dot{\varphi}(\tau) + \omega_o) = \frac{2\pi}{n} \tag{5.4}$$

$$\Leftrightarrow \tau_n(\tau) \approx \frac{2\pi}{n(\omega_o + \dot{\varphi}(\tau))}. \tag{5.5}$$

It should be noted that this approximation is no longer valid when the bit is in the torsional stick phase (i.e., when $\omega_o + \dot{\varphi}(\tau) \approx 0$). See Figure 8 for a comparison between the real delay τ_n and the approximation in (5.5).

By combining the results obtained in section 4.2 and the approximation (5.5), we can construct an analytical approximation $G_a(\omega_o + \dot{\varphi}(\tau))$ of $\langle g(\dot{u}(\tau, \tau_n))\rangle_a$ that is valid when the axial limit cycle exists and is stable ($\bar{\tau}_n > \pi - 1 \Leftrightarrow \omega_o + \dot{\varphi}(\tau) < \omega_o^s$ and $\mathcal{W}_o/\lambda < 2$):

$$G_a(\omega_o + \dot{\varphi}(\tau)) = \frac{(\mathcal{W}_o - \lambda)}{\lambda} \frac{\left(2\pi\sqrt{\psi} - (\pi-1)\sqrt{n(\omega_o + \dot{\varphi}(\tau))}\right)}{2\pi\sqrt{\psi} + \pi\sqrt{n(\omega_o + \dot{\varphi}(\tau))}}. \tag{5.6}$$

By substituting $G_a(\omega_o + \dot{\varphi}(\tau))$ into (5.3), we obtain an approximate equation governing the slow torsional vibrations

$$\ddot{\varphi}(\tau) + \varphi(\tau) = -n(1-\beta)\lambda_n G_a(\omega_o + \dot{\varphi}(\tau)) \tag{5.7}$$

that becomes autonomous and nonlinear because of the term $G_a(\omega_o + \dot{\varphi}(\tau))$. This equation (or reduced model) will be helpful to characterize the origin and the nature of torsional vibrations.

The following observations are drawn from (5.6):

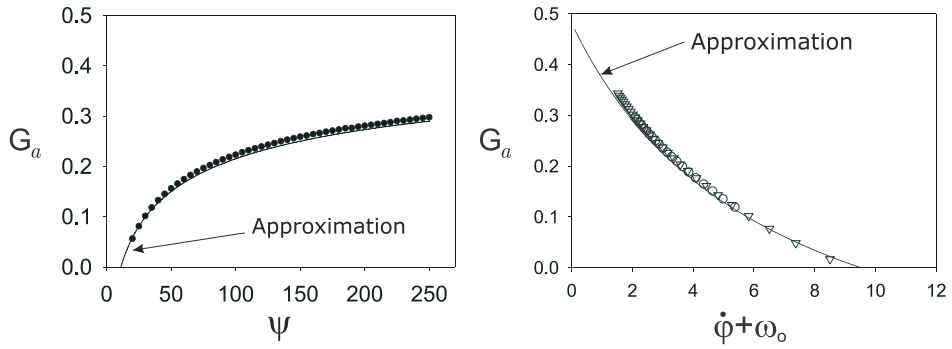

Figure 9. *Left:* G_a *with respect to* ψ *when* $n = 6$, $\omega_o+\dot{\varphi}(\tau) = 4$, $\mathcal{W}_o = 8$, *and* $\lambda = 5.4$. *Right:* $G_a(\omega_o+\dot{\varphi}(\tau))$ *with respect to* $\omega_o + \dot{\varphi}(\tau)$ *for three different values of* $\omega_o(1, 3, 6)$. *The bifurcation between the stable axial limit cycle and the stable axial equilibrium occurs at* $2\sqrt{2\psi/n} = 9.17$ *in this example.*

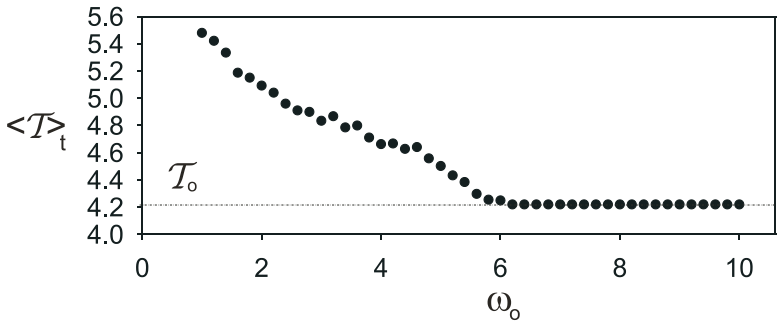

Figure 10. *Torque averaged over several bit revolutions for different values of the rotational speed obtained from numerical simulations of the complete system.*

- $G_a\left(\omega_o + \dot{\varphi}\left(\tau\right)\right)$ is monotonically increasing with the parameter ψ (see left panel in Figure 9) for all other parameters fixed.
- In Figure 9, $G_a\left(\omega_o + \dot{\varphi}\left(\tau\right)\right)$ is plotted for different values of $\omega_o + \dot{\varphi}\left(\tau\right)$. When $\omega_o + \dot{\varphi}\left(\tau\right) > \omega_o^s$, then $G_a\left(\omega_o + \dot{\varphi}\left(\tau\right)\right) = 0$, which corresponds to the exponential local stability of the axial equilibrium point. The monotonic decrease of $G_a\left(\omega_o+\dot{\varphi}\left(\tau\right)\right)$ with $\omega_o + \dot{\varphi}\left(\tau\right)$ recovers the so-called velocity weakening law, often empirically assumed to be an intrinsic property of the bit-rock interaction (see [3, 4]) and the essential cause of the torsional vibrations. In the present model, the velocity weakening law is a consequence of the axial vibrations and more precisely of the decreases of the contact forces occurring at the wearflat-rock interface. The velocity weakening effect in the torque is further illustrated in Figure 10.
- The function $G_a\left(\omega_o+\dot{\varphi}\left(\tau\right)\right)$ is directly proportional to $\mathcal{W}_o/\lambda-1 = n\bar{v}_o\bar{\tau}_{no}/\lambda$, which is the cumulative nominal dimensional depth of cut scaled by the dimensionless frictional contact.

5.2. Local stability analysis. By using the approximate analytical expression of G_a in (5.6), we can perform a local stability analysis of the equilibrium point of the reduced model.

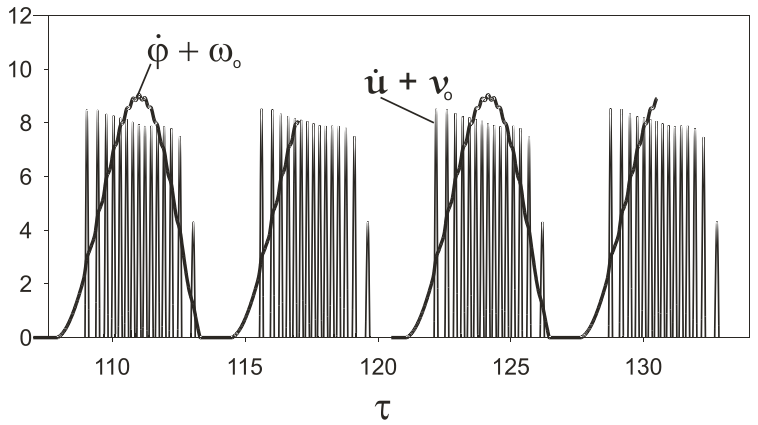

Figure 11. *Stick-slip torsional and axial vibrations. The frequency of the torsional dynamics $\dot{\varphi}$ differs strongly from the axial dynamics $\dot{u}$ ($n = 6$, $\psi = 63.1$, $\beta = 0.276$, $\omega_o = 4$, $\mathcal{W}_o = 3.44$).*

Jacobian linearization of the model yields

$$\ddot{\varphi}(\tau) - (1-\beta)\lambda G_a'(\omega_o)\dot{\varphi}(\tau) + \varphi(\tau) = -(1-\beta)\lambda G_a(\omega_o), \tag{5.8}$$

with

$$G_a'(\omega_o) = \left.\frac{dG_a(\omega)}{d\omega}\right|_{\omega=\omega_o} = -(2\pi-1)\frac{(\mathcal{W}_o/\lambda - 1)\,2\sqrt{n\psi}}{\pi\left[2\sqrt{n\psi} + n\omega_o\right]^2}. \tag{5.9}$$

The bits commonly used in the petroleum industry are characterized by $\beta < 1$. Since $\mathcal{W}_o > \lambda$ (a necessary condition for drilling), we can conclude the following:

1. The equilibrium point of (5.7) is given by
$$\varphi(\tau) = -(1-\beta)\lambda G_a(\omega_o) \quad \text{and} \quad \dot{\varphi}(\tau) = 0. \tag{5.10}$$
It thus depends on the fast axial dynamics ($G_a(\omega_o)$).
2. The derivative $G_a'(\omega_o)$ is always negative when $\bar{\tau}_n \approx 2\pi\sqrt{n\psi}/n\,(\omega_o + \dot{\varphi}(\tau)) > \pi - 1$, meaning that equilibrium point in torsion is unstable.
3. $\bar{\tau}_n \approx 2\pi\sqrt{n\psi}/n\,(\omega_o + \dot{\varphi}(\tau)) < \pi - 1$, $G_a'(\omega_o) = 0$, and the reduced model reduces to a harmonic oscillator. Then, the equilibrium point of the reduced model is marginally stable. Marginal stability of the reduced model gives rise to the quasi-limit cycle discussed in section 5.4.

5.3. Large torsional vibrations. Large torsional vibrations are observed when the axial dynamics exhibits a stable limit cycle with stick and slip phases. These torsional oscillations are characterized by a fast growth of the amplitude of the torsional vibrations and under certain conditions a large torsional limit cycle that exhibits alternating stick ($\dot{\varphi} = -\omega_o$) and slip phases ($\dot{\varphi} > -\omega_o$). The dominant frequencies occurring in the axial and torsional modes differ strongly (see Figure 11).

The local stability analysis of the analytical approximation of the reduced model predicts that the torsional oscillations will appear when $2\pi\sqrt{n\psi}/n\,(\omega_o + \dot{\varphi}(\tau)) > \pi - 1$. The numerical

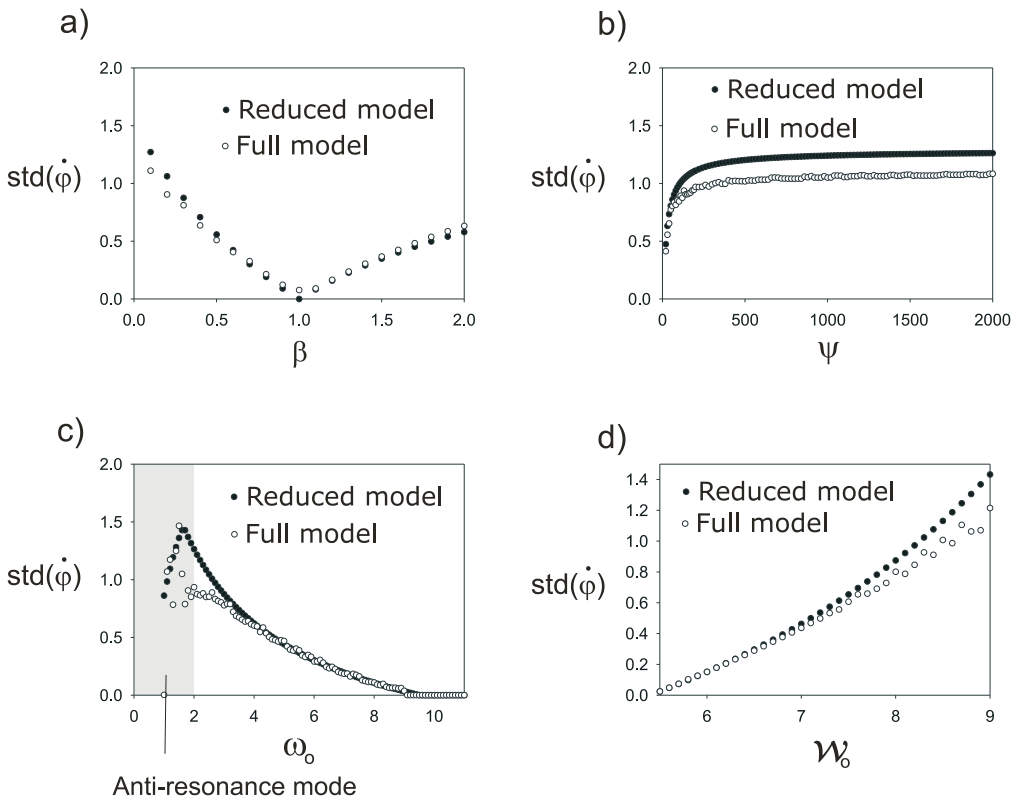

Figure 12. *Comparison between the standard deviation of the solution $\dot{\varphi}$ of the full model and the approximated reduced model with $n = 6$, $\beta = 0.3$, $\psi = 63.1$, $\mathcal{W}_o - \lambda = 2.6$, $\omega_o = 3$ obtained through numerical simulation with a simulation time $T = 5$.*

solutions of the analytical approximation of the torsional system and the numerical solutions of the full model are compared by measuring the standard deviation of the bit angular velocity around its nominal value, defined as

$$\mathrm{std}(\dot{\varphi}) = \frac{1}{T}\int_0^T \dot{\varphi}^2(t)\mathrm{d}t.$$

In Figure 12, we have arbitrarily chosen initial conditions at rest for both systems ($\varphi(0) = \dot{\varphi}(0) = 0$). The deviation of the initial condition from the equilibrium is thus given by $-(1-\beta)\,\lambda G_a\,(\omega_o)$ (see (5.10)). The effect of the magnitude of the initial deviation is mainly observed when the simulation time T is relatively short ($T = 5$). The full model and the reduced model are in good agreement except for the so-called antiresonance zone, which will be briefly discussed in section 6.1. We see, for instance, that the results in Figure 12(b) and 12(c) are consistent with the results presented in Figure 9.

In Figure 13, the simulations are initialized near the equilibrium value of the reduced model (see (5.10)). The initial condition on the bit rotational velocity $\dot{\varphi}\,(0)$ is set to $10^{-3}\omega_o$ in order to trigger the oscillations in the analytical approximation of the torsional dynamics. There again, we observe coherent numerical results between the two models.

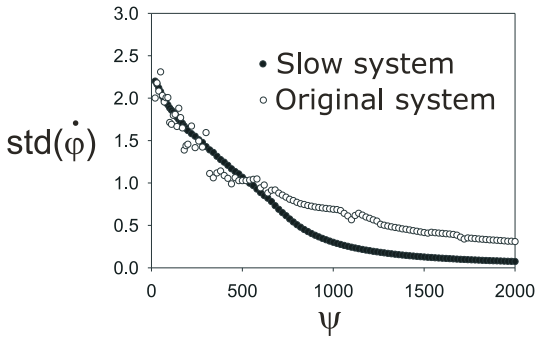

Figure 13. *Comparison between the standard deviation of the solution $\dot{\varphi}$ of the original and slow systems with $n = 6$, $\beta = 0.3$, $\psi = 63.1$, $\mathcal{W}_o - \lambda = 2.6$, $\omega_o = 3$ obtained through numerical simulation with a simulation time $T = 130$.*

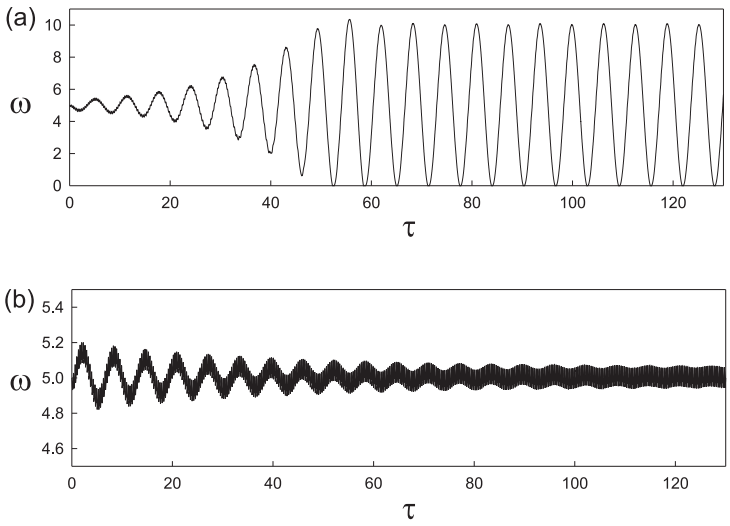

Figure 14. *Different types of evolution of the torsional vibrations when $n = 6$, $\psi = 50$, $\mathcal{W}_o - \lambda = 2$, $\omega_o = 5$;* (a) $\beta = 0.3$, (b) $\beta = 1.3$*; after* [18].

It should be emphasized that the amplitude of the torsional limit cycle in the full model may depend on the initial condition. Although the numerical simulations usually match the rate of growth of the oscillations predicted with the reduced equation (5.7), the torsional limit cycles may differ slightly. Nevertheless, the vibrations remain large and can be considered as detrimental for the drillstring.

Our analysis identifies the mean effect of axial vibrations $G_a(\omega_o + \dot{\varphi}(\tau))$ as a critical damping term in the torsional dynamics. Inspection of $G_a(\omega_o + \dot{\varphi}(\tau))$ provides simple recommendations for the drillers: a parameter $\beta > 1$ guarantees positive damping, i.e., the absence of stick-slip vibrations, as seen in Figure 14. Furthermore, geometric parameters should be designed to minimize the term $(1 - \beta)\lambda G_a'(\omega_o)$.

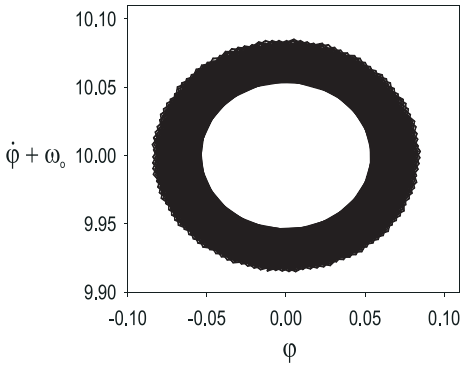

Figure 15. *Quasi-limit cycle in the phase plane* $(\varphi, \dot{\varphi})$. *The parameters are* $n = 6$, $\psi = 63.1$, $\beta = 0.276$, $\omega_o = 10$, $\mathcal{W}_o - \lambda = 3.44$.

5.4. Quasi-limit cycle. A quasi-limit cycle is observed when the axial equilibrium is stable and when the function $G_a(\omega_o + \dot{\varphi}(\tau))$ in (5.6) vanishes, resulting in the reduced dynamics $\ddot{\varphi}(\tau) + \dot{\varphi}(\tau) = 0$.

Figure 15 depicts a cross section of the phase diagram $(\varphi, \dot{\varphi})$ in this regime. Each loop takes about 2π units of dimensionless time. The amplitude of the torsional limit cycle strongly depends on the initial conditions. Although the right-hand side of (5.7) is zero, we observe a slow amplification of the torsional vibrations in the full model (see Figure 15). The marginal stability of the reduced model is inconclusive for the stability of the global system.

It should be emphasized that the damping term in (5.8) is destabilizing when $\beta < 1$, unless $G_a'(\omega_o) = 0$, which characterizes the just described quasi-limit cycle regime. It is seen in Figure 10 that this parametric condition will occur for ω_o sufficiently large. The consequence is that increasing the rotational speed is a way to avoid the exponential instability of the torsional equilibrium when $\beta < 1$. This is consistent with field practice where drilling structures are often equipped with a down-hole motor.

6. Limitations of the two-time-scales approach. The two-time-scales approach in the previous section provides an accurate prediction of the different behaviors of the model in parametric regions when there is a clear separation between the fast time scale of axial dynamics and the slow time scale of torsional dynamics.

In this section, we briefly describe additional phenomena that are observed when this time scale separation no longer holds.

6.1. Antiresonance. The antiresonance regime occurs when the axial dynamics exhibit stick-slip oscillations that eventually damp the torsional vibrations. It occurs mainly at very low nominal rotational speeds ω_o, as seen in Figure 16.

In order to understand the source of this destabilizing mechanism, we simulated the axial dynamics while imposing $\dot{\varphi}$ as a harmonic signal of amplitude $\omega_o/2$. Figure 17 illustrates the evolution of $\lambda_n g(\dot{u})$ at two different speeds:

- on the left, $\omega_o = 1$, and the antiresonance phenomenon occurs;
- on the right, $\omega_o = 3$, and the torsional stick-slip oscillations are fully developed.

The antiresonance process is clearly identified as a synchronization of the amplitude of

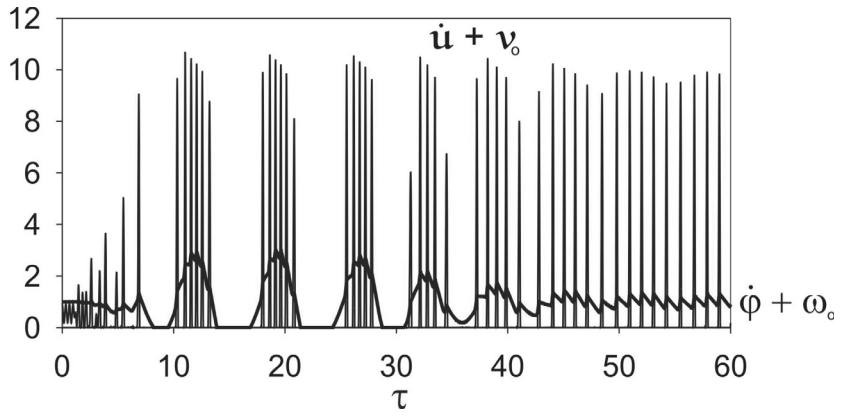

Figure 16. *Antiresonance regime: Torsional vibrations are stabilized by the axial vibrations* ($n = 6$, $\psi = 63.1$, $\beta = 0.276$, $\omega_o = 1$, $\mathcal{W}_o - \lambda = 3.44$).

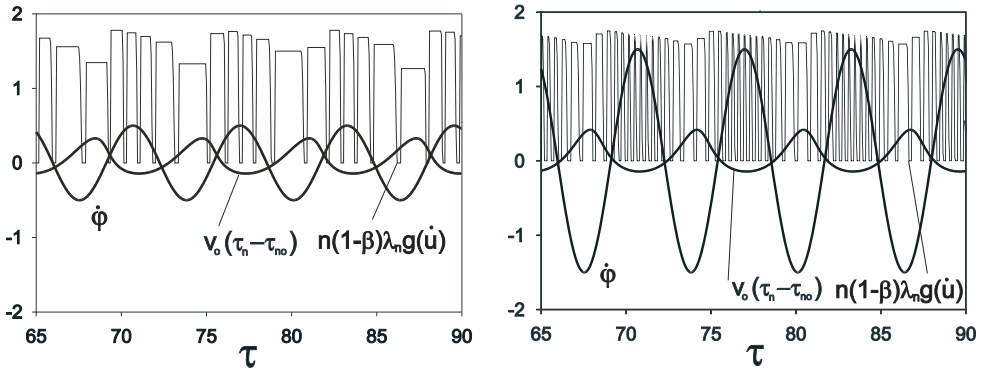

Figure 17. *Evolution of* $v_o\,(\tau_n - \tau_{no})$ *and* $n(1-\beta)\lambda_n g(\dot{u})$ *when the angular bit velocity* $\dot{\varphi} + \omega_o$ *is imposed to be harmonic and with a bias of* $\omega_o/2$. *On the left, the rotational speed* ω_o *is such that we observe numerically the antiresonance mode, while on the right, the steady state corresponding motion is stick-slip vibrations in torsion.*

the plateaus of $g(\dot{u})$ with the angular velocity, stabilizing the torsional equilibrium at hand.

This particular stabilization mechanism of the torsional equilibrium occurring at small ω_o is not predicted by the two-time-scales approach. Furthermore, the two-time-scales approach predicts that the amplitude of the axial limit cycle is influenced only by $v_o\tau_{no}$ and not by τ_n (see Figure 18). However, the variation of the amplitude of the plateaus of $g(\dot{u})$ with the angular velocity or equivalently the delay τ_n is clearly noticeable in Figure 17. Figure 19 suggests that the variation of the delay during the axial slip phase, i.e., when $g(\dot{u}) = 0$, is a passive source of the stability mechanism. In Figure 19, the delay is first constant and then increases linearly. Therefore, the variation of the magnitude of the plateaus of $g(\dot{u})$ depends on the slope of τ_n during the axial slip phase. As a matter of fact, the axial dynamics act as a sampler of the derivative of the delay at each slip phase. The value of the derivative of the delay at these particular instants affects the height of the plateaus of $g(\dot{u})$. The maximum values of $n(1-\beta)\lambda_n g(\dot{u})$ are plotted in Figure 20 for different values of the slope of τ_n.

The antiresonance regime is advantageous because it stabilizes the torsional equilibrium.

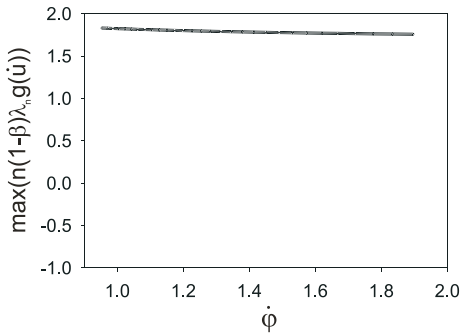

Figure 18. *Evolution of the maximum value of* $n\,(1-\beta)\,\lambda_n g(\dot{u})$ *over one axial limit cycle for different values of* $\dot{\varphi}$ *obtained with the shooting method (we use the approximation* $\dot{\varphi} \approx \frac{2\pi}{n\tau_n} - \omega_o$*).*

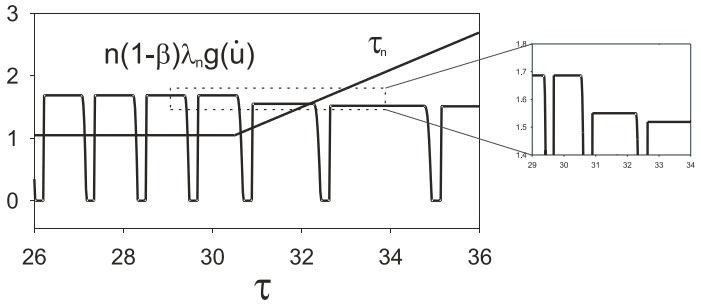

Figure 19. *Evolution of* τ_n *and* $n\,(1-\beta)\,\lambda_n g(\dot{u})$ *when the delay changes as an increasing ramp.*

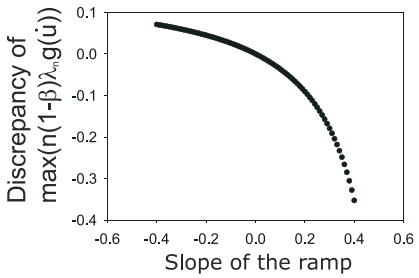

Figure 20. *Discrepancy of* $\max(n\,(1-\beta)\,\lambda_n g(\dot{u}))$ *for different slopes of ramp of* τ_n*.*

Unfortunately, it occurs only at extremely low rotational speed, which makes it an impractical solution in drilling applications.

6.2. Delayed bifurcations.

6.2.1. Bit bouncing. The analysis in section 4.3 predicted bit bouncing when the axial equilibrium is unstable and the axial limit cycle does not exist, i.e., $\bar{\tau}_n > \pi/\sqrt{2}$ and $\mathcal{W}_o > 2\lambda$ (see Figure 7).

When the bit experiences torsional vibrations, $\dot{\varphi}\,(\tau)$ oscillates around zero, and it may happen that the delay $\bar{\tau}_n\,(\tau) \approx 2\pi\sqrt{\psi}/\sqrt{n}\,(\omega_o + \dot{\varphi}\,(\tau))$ oscillates around $\pi/\sqrt{2}$. This occurs

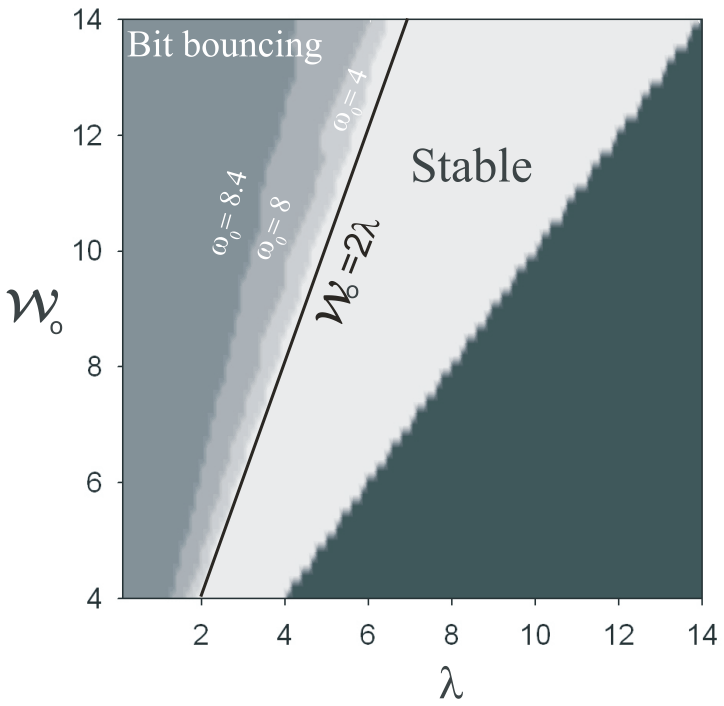

Figure 21. *Map of stability for different rotational speeds* ω_o ($n = 6$, $\beta = 0.276$, $\psi = 63.1$)*; after* [9].

when ω_o approaches the bifurcation value $\omega_o^s = 2\sqrt{2\psi/n}$.

The asymptotic solutions of the (delay-frozen) fast axial dynamics then alternate between stable and unstable axial equilibrium. In the full model, this phenomenon delays the bit bouncing bifurcation predicted at $\mathcal{W}_o = 2\lambda$. Figure 21 illustrates that the transition from stable drilling to bit bouncing in the full model moves away from the theoretical prediction $\mathcal{W}_o = 2\lambda$ as ω_o approaches the bifurcation value $\omega_o^s = 2\sqrt{2\psi/n} = 9.17$. This effect is also visible in Figure 7.

6.2.2. Quasi-limit cycle. For the same reason, the results obtained for the reduced model and for the full model may differ when the parameters are in the vicinity of the bifurcation $\omega_o^s = 2\sqrt{2\psi/n}$, as displayed in Figure 22. The parametric region where a quasi-limit cycle is observed in numerical simulations is much larger than the one predicted from the reduced model. This is because the transient time to pass from the axial equilibrium point to the stable axial limit cycle is not negligible. The fast axial solutions do not reach steady state over this time frame, which reduces the averaged frictional term $\lambda_n \langle g(\dot{u}(\tau)) \rangle_a$ and therefore delays the instability of the torsional dynamics.

7. Conclusions. A novel approach to modeling stick-slip vibrations of drag bits in drilling structures accounts for the coupling between the axial and the torsional modes of vibrations via the bit-rock interface laws. This coupling introduces a state-dependent delay and a discontinuous friction term in the governing equations. Numerical simulations (see [18]) show the

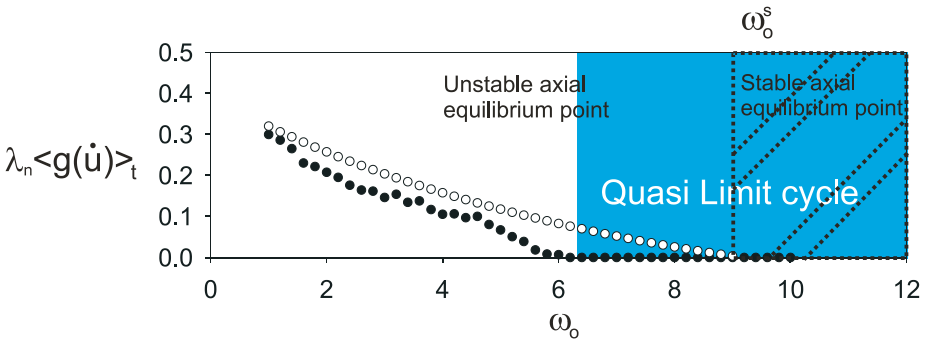

Figure 22. *Mean value of the friction term over one limit cycle in torsion* ($\lambda_n \langle g(\dot{u})\rangle_t = \frac{\lambda_n}{T}\int_0^T g(\dot{u})\mathrm{d}t$) *in terms of* ω_o. *The black dots are the solutions of the full model, while the white dots are the solutions of the fast subsystem.*

existence of different steady-state behaviors, such as axial and torsional stick-slip oscillations, antiresonance regime of the torsional dynamics, and a quasi-limit cycle or bit bouncing, in the torsional or axial direction, respectively. Furthermore, a parametric analysis reveals that the apparent decrease of the mean torque with the angular velocity responsible for the growth of the amplitude of the torsional vibrations is a consequence of the axial vibrations and more precisely of the intermittent decreases of the frictional contact forces at the wearflat-rock interface.

The dimensionless formulation exhibits a large parameter ψ in the model, which enables a two-time-scales analysis of the axial and torsional dynamics. The axial mode oscillates much faster than the torsional mode of vibration. In this paper, we present an asymptotic analysis that decouples fast axial dynamics (with a frozen constant delay) from the slow torsional dynamics, influenced only by the averaged behavior of the fast dynamics. When the delay is larger than a critical value $\pi/\sqrt{2n\psi}$, where n is the number of blades mounted on the bit, a stable limit cycle in the axial direction is observed over a certain parametric range. An approximate model of the axial dynamics is proposed to provide an analytical characterization of the limit cycle. The resulting analytical predictions match the numerical observations well. They are useful for characterizing the phenomenon of bit bouncing, which originates from the instability of the axial solutions.

The approximate model also provides an analytical expression of the averaged reacting torque-on-bit that influences the torsional dynamics. Its variation in terms of the bit angular velocity recovers the empirical velocity weakening law observed in experiments. The analysis of the slow torsional dynamics predicts the emergence of the different regimes of torsional vibrations (stick-slip vibrations or a quasi-limit cycle) in parametric ranges that agree with the numerical simulations. The analytical predictions provide useful recommendations for the design of drilling structure, the selection of the operating parameters, or the control synthesis.

We also discuss some limitations of the two-time-scales approach to capturing phenomena such as antiresonance or delayed bifurcations. The antiresonance regime is characterized by small vibrations of the bit angular velocity around its nominal value, although the bit experiences intermittent losses of frictional contact. This regime occurs at low rotational speed, or equivalently at large delay. It is only observable when the axial stick time is large

enough to generate phase locking with the bit angular velocity.

This work possibly opens new perspectives for the synthesis of passive control laws to reduce the amplitude of the torsional vibrations. Most notably, it was shown that the equilibrium of the torsional dynamics could become exponentially stable by changing the bit design through the parameter β or the number of active blades n.

Acknowledgments. This paper presents research partially supported by the Belgian Programme on Inter-university Poles of Attraction, initiated by the Belgian State, Prime Minister's Office for Science, Technology and Culture.

This research was initiated at the University of Minnesota under the supervision of Pr. Emmanuel Detournay through the Ph.D. thesis of Dr. Thomas Richard and the M.Sc. thesis of Christophe Germay. The authors would also like to thank Pr. Emmanuel Detournay for his careful review of the manuscript.

REFERENCES

[1] J. I. Adachi, E. Detournay, and A. Drescher, *Determination of rock strength parameters from cutting tests*, in Proceedings of the 2nd North American Rock Mechanics Symposium (NARMS 1996), Rotterdam, 1996, Balkema, Leiden, The Netherlands, 1996, pp. 1517–1523.

[2] R. Almenara and E. Detournay, *Cutting experiments in sandstones with blunt PDC cutters*, in Proceedings of the International Society of Rock Mechanics Symposium EuRock '92, Thomas Telford, London, 1992, pp. 215–220.

[3] J. F. Brett, *The genesis of torsional drillstring vibrations*, SPE Drill. Eng., September (1992), pp. 168–174.

[4] N. Challamel, *Rock destruction effect on the stability of a drilling structure*, J. Sound Vibration, 233 (2000), pp. 235–254.

[5] C. Canudas de Wit, H. Olson, K. J. Astrom, and P. Lischinsky, *A new model for control of systems with friction*, IEEE Trans. Automat. Control, 40 (1995), pp. 419–425.

[6] E. Detournay and P. Defourny, *A phenomenological model of the drilling action of drag bits*, Int. J. Rock Mech. Min. Sci. & Geomech. Abstr., 29 (1992), pp. 13–23.

[7] R. P. H. Faassen, N. Van de Wouw, J. A. J. Oosterling, and H. Nijmeijer, *Prediction of regenerative chatter by modeling and analysis of high-speed milling*, Internat. J. Machine Tool and Manufacture, 43 (2003), pp. 1437–1445.

[8] A. F. Filippov, *Differential equations with discontinuous right-hand side*, Amer. Math. Soc. Transl., 42 (1964), pp. 199–231.

[9] C. Germay, *Self-Excited Vibrations of Drag Bits*, Master's thesis, University of Minnesota, 2002.

[10] T. Insperger, G. Stepan, and J. Turi, *State dependent delay model for regenerative cutting processes*, in Proceedings of the Fifth EUROMECH Nonlinear Dynamics Conference (ENOC 2005), Eindhoven, The Netherlands, 2005, pp. 1124–1129.

[11] J. Jansen, L. van den Steen, and E. Zachariasen, *Active damping of torsional drillstring vibrations with a hydraulic top drive*, SPE Drilling Completion, 10 (1995), pp. 250–254.

[12] R. I. Leine, D. H. van Campen, and W. J. G. Keultjes, *Stick-slip whirl interaction in drillstring dynamics*, J. Vibration Acoustics, 124 (2002), pp. 209–220.

[13] N. Mihajlovic, A. A. van Veggel, N. van de Wouw, and H. Nijmeijer, *Analysis of friction induced limit cycling in an experimental drill-string system*, J. Dynam. Systems Measurement and Control, 126 (2004), pp. 709–720.

[14] E. M. Navarro-Lopez and R. Suarez-Cortez, *Practical approach to modelling and controlling stick-slip oscillations in oilwell drillstrings*, in Proceedings of the IEEE International Conference on Control Applications, 2004, IEEE Press, Piscataway, NJ, pp. 1454–1460.

[15] T. S. Parker and L. O. Chua, *Practical Numerical Algorithms for Chaotic Systems*, Springer-Verlag, New York, 1989.

[16] D. R. Pavone and J. P. Desplans, *Application of high sampling rate downhole measurements for analysis and cure of stick-slip in drilling*, in Proceedings of the SPE Annual Technical Conference and Exhibition, 1994, SPE 28324, pp. 335–345.
[17] T. Richard, C. Germay, and E. Detournay, *Self-excited stick-slip oscillations of drill bits*, C. R. Mécanique, 332 (2004), pp. 619–626.
[18] T. Richard, C. Germay, and E. Detournay, *Self-excited vibrations of drilling systems with drag bits*, J. Sound Vibration, 305 (2007), pp. 432–456.
[19] A. F. A. Serrarens, M. J. G. van de Molengraft, J. J. Kok, and L. van den Steen, *H*1 *control for suppressing stick-slip in oil well drillstrings*, IEEE Control Systems Mag., 18 (1998), pp. 19–30.
[20] G. Stepan, *Delay-differential equation models for machine tool chatter*, in Dynamics and Chaos in Manufacturing Processes, F. C. Moon, ed., Wiley, New York, 1998, pp. 165–191.
[21] A. R. Teel, L. Moreau, and D. Nesic, *A unified framework for input-to-state stability in systems with two time scales*, IEEE Trans. Automat. Control, 48 (2003), pp. 1526–1544.
[22] J. Tlusty and M. Polacek, *The stability of machine tool against self-excited-vibrations in machining*, in Proceedings of the ASME Production Engineering Research Conference, American Society of Mechanical Engineers, New York, 1963, pp. 465–474.